Celal Bayar University Journal of Science
Volume 17, Issue 3, 2021, p 285-295
Doi: 10.18466/cbayarfbe.887714

Celal Bayar University Journal of Science

Synthesis, Spectroscopic Characterization, Crystal Structure and Theoretical Studies on New Organic Single Crystal of 1-(3,5-Difluorophenyl)-3-(2-Nitrophenyl)Urea

Tuğba Güngör[1]*, Tuncay Karakurt[2], Zarife Sibel Şahin[3]

[1] Department of Chemistry, Faculty of Sciences and Arts, Natural Products and Drug Research Laboratory, Çanakkale Onsekiz Mart University, Çanakkale, Turkey
[2] Department of Chemical Engineering, Faculty of Engineering-Architecture, Kırsehir Ahi Evran University, Kırsehir, Turkey
[3] Department of Energy Systems Engineering, Faculty of Engineering and Architecture, Sinop University, Sinop, Turkey
*tgungor@comu.edu.tr
*Orcid: 0000-0001-5261-1856

Received: 27 February 2021
Accepted: 1 June 2021
DOI: 10.18466/cbayarfbe.887714

Abstract

A new organic compound, 1-(3,5-difluorophenyl)-3-(2-nitrophenyl)urea was synthesized from 2-nitroaniline, 3,5-difluoroaniline and triphosgene in sequential two steps with 92% yield. The product was crystallized by the slow evaporation using THF and ethyl acetate solvent system to obtain its single crystal. The pure crystals were characterized with melting point, FT-IR, ^{1}H NMR, ^{13}C NMR and MS. The structure of the compound was brought to light by X-ray single-crystal structure determination. Density functional theory calculations were applied by using (DFT/B3LYP) method with the 6-311G(d,p) basis set level. The potential energy surface (PES) scanning was performed to determine the stability of the molecule. Frontier molecular orbitals of the compound were calculated. AIM charge and MEP analyzes were performed.

Keywords: Crystal structure, DFT calculations, diphenylurea, triphosgene, XRD

1. Introduction

In recent years, there has been an increasing interest in 1,3-diphenylureas which are also known as *N,N'*-diphenylureas due to their wide range of chemical and biological applications [1,2]. It is known that these compounds show good pharmacological activities including anticancer [3-5], antimalarial [6,7], anti-Alzheimer [8], antiviral [9], carbonic anhydrase I and II inhibitors [2], anti-tuberculosis [10] and antidepressant [11,12]. Regorafenib named 4-(4-(((4-chloro-3-(trifluoromethyl)phenyl)carbamoyl}amino)-3-fluoro phenoxy)-*N*-methylpyridine-2-carboxamide which is a diphenylurea derivative drug shows the pharmaceutical properties as multikinase inhibitor of VEGFR-2, -3, c-Kit, p38 MAP kinase *etc.* and uses at the treatment of colorectal, hepatocellular and gastrointestinal stromal cancers [3]. In addition, sorafenib is another effective kinase inhibitor drug containing diphenylurea moiety uses for the treatment of kidney, liver and thyroid cancers [5]. Also, 1,3-diphenylureas were reported acting like auxins and cytokinins which are important plant growth regulators in agrochemical applications [13].

The synthesis of unsymmetrical diphenylurea derivatives is an important issue due to their superior biological applications and chemical treatments including usage as intermediate, linker in complex synthesis and also protection of amino groups. Synthesis of target structures can be carried out with aniline derivatives and phosgene [14,15], triphosgene (BTC, bis(trichloromethyl) carbonate) [16], 1,1'-carbonyldiimidazole (CDI) [7], *S,S*-dimethyl dithiocarbonate [17], 1,1-carbonylbis benzotriazole [18] or carbon monoxide/dioxide with catalysts [19,20] as CO sources. In addition, alternative synthesis method is Curtius rearrangement which begins with a different

starting material, substituted benzoyl chlorides. The first step of this method is the reaction of benzoyl chloride derivative and sodium azide to obtain benzoyl azide derivative. In the second step, *in situ* generation of isocyanate occurs through the removal of nitrogen gas and the reaction of aniline derivative with intermediate isocyanate results in the target diphenylurea product [21].

The density functional theory (DFT) is an approach that determines the quantum chemical model of structures and is presently one of the most successful methods. DFT predicts many molecular properties such as molecular structures, vibrational frequencies, molecular energies, and electric properties. The fact that the simulation results are very close to experimental studies is one of the reasons why DFT is a preferred method.

In this study, we synthesized a new *N,N'*-diphenylurea derivative (compound **4**) successfully using a two-step synthesis approach with high yield. The well-shaped crystals of product were obtained by using slow evaporation technique and characterized with melting point and various spectral analyses such as FT-IR, ^{1}H NMR, ^{13}C NMR, MS and X-ray single diffraction. Theoretical calculations were performed using the DFT(B3LYP) method and 6-311G(d,p) basis set to determine and characterize the molecular and electronic structure properties of the compound. NMR and IR values of the optimized structure were compared to the experimental values. The potential energy surface (PES) scanning was performed to determine the stability of molecule. Frontier molecular orbitals of the compound were calculated. Also, AIM charge and MEP analyzes were performed.

2. Materials and Methods

All chemicals and solvents used in the experimental studies were provided from commercial suppliers and used without further purification. Reaction tracking was conducted by using thin-layer chromatography with Merck precoated Kieselgel 60GF$_{254}$ plates. Melting point was recorded with X-4 melting-point apparatus. Infrared spectra were measured with a Perkin Elmer Spectrum 100 FTIR spectrophotometer in the range 4000-600 cm^{-1} with attenuated total reflectance (ATR) sampling accessory. NMR spectra were registered with a Jeol High-Performance Digital FT-NMR spectrometer (400 and 100 MHz for ^{1}H and ^{13}C, respectively) using DMSO-d$_6$ as solvent. The molecular weight of product was determined with Shimadzu LC-MS/MS 8040 Liquid Chromatograph Mass Spectrometer with an ESI source. The single crystal X-ray diffraction (XRD) data was collected at ambient temperature on an Agilent Supernova X-Ray Diffractometer using Molybdenum X-ray source and CCD detector. Literature search of compound was done using Reaxys database.

2.1. Synthesis of 1-(3,5-difluorophenyl)-3-(2-nitrophenyl)urea (compound 4)

2-Nitroaniline (**1**, 1.0 mmol; 0.138 g) was dissolved in 2 mL DCM. Bis(trichloromethyl)carbonate (triphosgene, 1.0 mmol; 0.296 g) in 1 mL DCM and triethylamine (0.3 mL) were added slowly in an ice bath. The mixture was stirred at 0-5 °C for 30 min and then room temperature for 2 hours. Solvent was evaporated in vacuo to dryness and the residue **(2)** was dissolved in a mixture of THF:DCM (1:1, 6 mL). 3,5-Difluoroaniline (**3**, 1.0 mmol; 0.129 g) was added to the reaction medium and was stirred at reflux condition for 4 hours. Upon completion as shown by TLC, solvent mixture was evaporated in vacuo to dryness. Crude product was dissolved in acetone (8 mL) and distilled water (8 mL) was added on it. Obtained orange solid was filtered, washed with water (20 mL) and dried at room temperature. (0.27 g, 92% yield) mp 200-202 °C; IR (ATR) ϑ 3404, 3332, 3127, 3098, 1728, 1630, 1605, 1502, 1477, 1415, 1335, 1269, 1168, 1140, 1113, 1087, 1047, 1002, 975, 872, 850, 837, 746, 706, 666 cm^{-1}; ^{1}H NMR (400 MHz, DMSO-d$_6$) δ 10.15 (s, 1H), 9.60 (s, 1H), 8.18 (dd, J= 8.45 and 1.15 Hz, 1H), 8.06 (dd, J= 8.33 and 1.45 Hz, 1H), 7.69 (td, J= 7.86 and 1.53 Hz, 1H), 7.22 (td, J= 7.80 and 1.26 Hz, 1H), 7.14 (dd, J= 9.87 and 2.25 Hz, 2H), 6.82 (tt, J= 9.39 and 2.31 Hz, 1H); ^{13}C NMR (100 MHz, DMSO-d$_6$) δ 164.41 and 164.26 (d, J_{C-F}=15.65 Hz), 161.99 and 161.84 (d, J_{C-F}=15.42 Hz), 152.26, 142.64-142.36 (t, J_{C-F}=13.96 Hz), 138.82, 135.50, 134.63, 125.95, 123.44, 101.97 and 101.68 (d, J_{C-F}=29.28 Hz), 98.27-97.75 (t, J_{C-F}=26.28 Hz); MS (ESI): m/z (%) 294 (M^+, 100), 279 (44), 163 (36).

2.2. Growth of Crystal

A saturated solution of product was prepared from the pure solid using THF as solvent and filtered. Vapor diffusion technique which use volatile-less volatile binary solvent system for better crystallization was applied to get single crystals. For this purpose, ethyl acetate was used as outer solvent and the solution was kept at room temperature. The orange needle crystals suitable for single-crystal diffraction experiments were obtained after ten days.

2.3. X-Ray Diffraction Analysis

Suitable crystal of compound **4** was selected for data collection which was performed on a SuperNova diffractometer equipped with a graphite-monochromatic Mo-K$_\alpha$ radiation at 296 K. The H atoms of C atoms were located from different maps and then treated as riding atoms with C-H distance of 0.93 Å. Other H atoms were located in a difference map and refined freely. We used these procedures for our analysis: solved by direct methods; SHELXS-2013 [22]; refined by full-matrix least-squares methods; SHELXL-2013

[23]; data collection: Bruker APEX2 [24]; molecular graphics: MERCURY [25]; solution: WinGX [26]. Details of data collection and crystal structure determinations were given in Table 3.

2.4. Theoretical Calculations

The molecular modeling studies of the compound were performed with the DFT/B3LYP method [27,28] and 6-311G(d,p) basis set [29] by using Gaussian 09 software package [30]. Aim charge analysis was done using AIMAII [31] suite of programs to examine intermolecular and intramolecular interactions. Molecular orbitals of the molecule were calculated and visualized using the Multiwfn program [32].

3. Results and Discussion

3.1. Synthesis of Title Compound

One-pot, sequential two-step synthesis was performed to the formation of target unsymmetrical urea derivative **4** (Figure 1). The first step was the synthesis of isocyanate intermediate **(2)** from 2-nitroaniline **(1)** and triphosgene by using triethylamine as base at room temperature. Mechanistically, triphosgene reagent causes to the by-product formation of 2 moles phosgene and HCl. While the reactive intermediate phosgene continues to the similar reaction with 2-nitroaniline to form isocyanate **2**, hydrochloric acid gives triethylammonium chloride with triethylamine base. Also, triethylamine helps to the removing of acidic hydrogens of -NH_2 group on 2-nitroaniline, increasing the nucleophilic power and accelerating the formation of the isocyanate **2**. The second step, a typical urea synthesis was carried out between intermediate **2** which was used directly without further purification and 3,5-difluoroaniline at reflux conditions in DCM/THF solvent mixture. As a result, 1-(3,5-difluorophenyl)-3-(2-nitrophenyl)urea **(4)** was obtained with high purity and high yield, 92% (Figure 1). Product was identified by melting point, FT-IR, ^{1}H NMR, ^{13}C NMR and LC-MS analyses (See experimental part and supplementary information). It is determined that compound is air-stable and soluble in common organic solvents such as acetone, ethyl alcohol, ethyl acetate, THF, DCM *etc.* but insoluble in water.

3.2. Spectroscopic Analysis

All spectra and data of the compound **4** were given in the Experimental part and Supplementary information. The calculated and experimental FT-IR spectrum and some of the compared characteristic frequencies were given in Figure 2 and Table 1. The compound has 84 normal modes of vibration (Table 1 and S1). The free vibration frequencies of the N–H group, which does not contain an intramolecular or intermolecular hydrogen bonding are in the range of 3700 and 3550 cm^{-1}, while the free vibration frequencies of the N–H group containing hydrogen bonding are observed in the range of 3200–2400 cm^{-1} [33]. In this study, the free vibration frequencies of the N-H mode of asymmetric ureas have been observed as 3404 and 3332 cm^{-1} experimentally, and this frequency is reported as 3179 cm^{-1} in the literature [34]. The calculated values were observed at 3476 and 3318 cm^{-1} with a contribution of 100 and 98% of PED (Potential Energy Distribution). In the presence of the N-H group which contains intermolecular or intramolecular hydrogen bonds within the molecule, the stretching vibration frequency values of this group decreased while the bending vibration frequency values increase [35]. The experimental/calculated values of the in-plane angle bending vibration frequency of N-H mode were obtained as 1630/1587-1485 cm^{-1}, while this value in literature is 1494 cm^{-1} [36]. The experimental/calculated values of the out-of-plane angle bending vibration frequency of N-H mode were obtained as 666/673 cm^{-1}.

Other major feature of compound was strong carbonyl (C=O) band at 1728 cm^{-1} and also this band appeared at 1714 cm^{-1} as pure strain vibration with 74% PED additive in the theoretical spectrum. The experimental band at 1502 and 1335 cm^{-1} corresponds to the asymmetrical and symmetrical stretching vibrations of the NO_2 group while N-O vibration frequencies (with PED additive) are calculated as 1595 (10%) cm^{-1}, 1541 (30%) cm^{-1}, 1435 (24%) cm^{-1}, 1313 (31%) cm^{-1} and 1252 (22%) cm^{-1}. Characteristic C-H vibration frequency values of aromatic compounds are observed in the range of 3100-3000 cm^{-1} [37], while C-C aromatic stretching vibrations are observed in the range of 1600-1400 cm^{-1} [38].

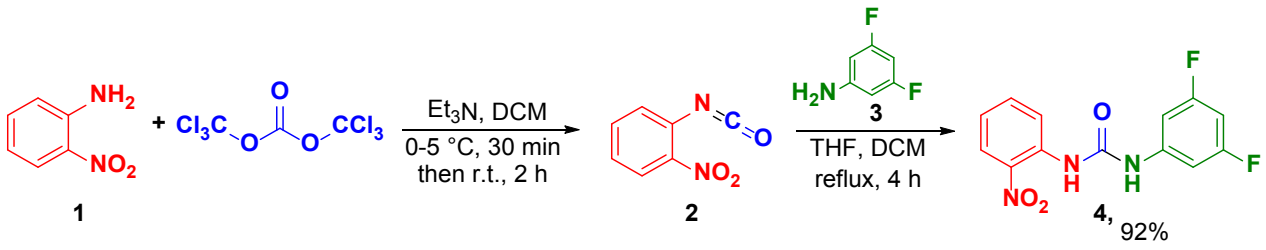

Figure 1. Two-step synthesis scheme of 1-(3,5-difluorophenyl)-3-(2-nitrophenyl) urea.

In our study, symmetrical C-H and C-C vibration frequencies were experimentally observed in the range of 3127, 3098 and 1605 cm^{-1}, respectively, and agree with the literature values 3110-3003 and 1666-1535 cm^{-1} [39].

Theoretically, C-H vibration frequency values (with PED contribution) were observed in 3134 (99%) cm^{-1}, 3126 (99%) cm^{-1}, 3106 (95%) cm^{-1}, 3102 (100%) cm^{-1}, 3076 (96%) cm^{-1}, 3066 (100%) cm^{-1} and 3056 (93%) cm^{-1} as pure C-H vibration while C-C mode was calculated as 1601 cm^{-1} with 45% of PED contribution. In-plane C-H angle bending vibration frequencies in the aromatic ring are experimentally observed between 1400–1000 cm^{-1} [40]. In our study, this vibration frequency was observed experimentally as 1477, 1415 cm^{-1} and calculated with the PED contributions theoretically as 1211 (26%) cm^{-1}, 1195 (55%) cm^{-1}, 1138 (66%) cm^{-1} and 1128 (30%) cm^{-1}. The stretching of the C-F bond was confirmed at 1113 cm^{-1} while this band appeared at 1092, 985, 953 cm^{-1} in the theoretical spectrum. Also, 1,2- and 1,3- C-H vibrations of di/trisubstitutedbenzene were determined as strong peaks at the fingerprint region (837 and 746 cm^{-1}) of experimental spectra. Other calculated vibration modes were given in Table S1.

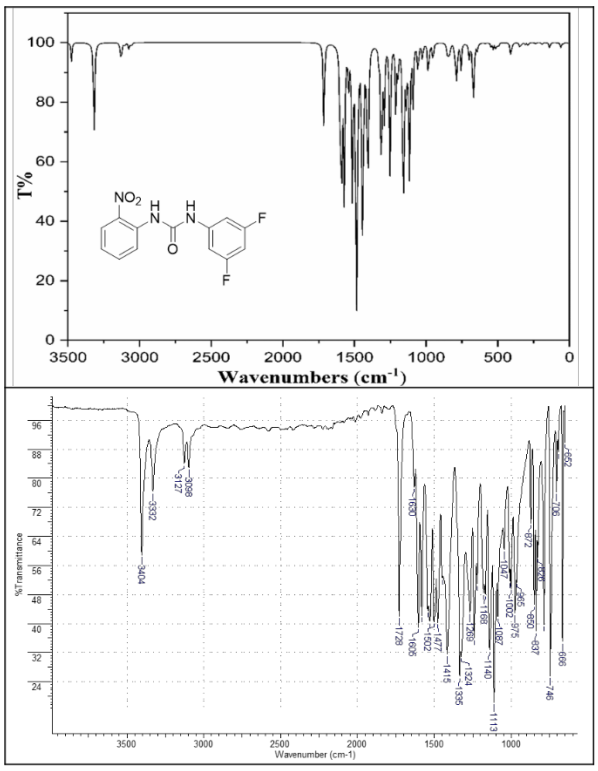

Figure 2. Theoretical and experimental IR spectra of the title compound.

To investigate NMR chemical shifts of the molecules, GIAO (Gauge-Independent Atomic Orbital) method [41,42] was used. ^{1}H and ^{13}C chemical shift values were calculated using the DFT/B3LYP method with 6-311G(d,p) basis set. The geometry of compound, together with that of tetramethylsilane (TMS, $Si(CH_3)_4$) were fully optimized choosing dimethyl sulfoxide (DMSO) solvent. The ^{1}H and ^{13}C NMR chemical shifts were converted to the TMS scale by subtracting the calculated absolute chemical shielding of TMS with values of 32.10 ppm (^{1}H) and 189.40 ppm (^{13}C). All ^{1}H and ^{13}C NMR peaks of compound **4** were monitored at the expected regions (Figure 3 and supplementary information) and confirmed the target structure (Table 2). When compound was examined spectroscopically in detail, signals were detected in the range of 10.15-6.82 ppm in ^{1}H NMR spectrum. Two characteristic broad singlet signals with 1H integration (10.15 and 9.60 ppm) confirm the presence of -NH groups of urea. The calculated shift values for these protons were found as 11.31 and 6.31 ppm. Four split peaks (H2-H5) with 1H integration on nitroaromatic ring (Ring A) were observed at 8.18, 8.06, 7.69 and 7.22 ppm and calculated as 9.37-7.16 ppm for theoretical spectrum. Also, three protons of fluoro atoms containing aromatic ring (Ring B) were shifted in the high-field of spectrum when compared Ring B. While doublet of doublets peak at 7.14 ppm corresponded to the protons H9 and H13 with 2H integration, the signal of H11 was appeared as triplets of triplet at 6.82 ppm due to splitting with two fluorine atoms in orto position and two hydrogen atom in meta position. In addition, these Ring B protons were calculated in the range of 8.31-6.38 ppm according to the DFT/6-311G(d,p) method.

In the ^{13}C NMR spectrum, the signal of carbonyl carbon of urea (C7) was located at 152.26 ppm and calculated as 153.11 ppm (Figure 3 and Table 2). Other aromatic carbons were observed in the region of 164.34-98.01 ppm as expected. The highest chemical shifts 164.34 and 161.92 ppm were belong to the fluorine-bound carbons C10 and C12 as doublet peaks because of the high deshielding effect of the electronegative fluorine atom. These carbons were found as 171.52, 170.83 ppm by theoretical calculations. However, the lowest value (98.01 ppm) which was splitted as a triplet peak by two neighbor fluorine atoms correspond to the C11 carbon and is calculated as 100.02 ppm. Also, triplet peak at 142.50 ppm was belong to carbon C8 and doublet peaks of 101.97 and 101.68 ppm were belong to the carbons C9 and C13. The chemical shifts of carbons C8, C9 and C13 were calculated as 146.96, 102.63 and 102.59 ppm, respectively. Carbons C1-C6 in the Ring A were observed at 134.63, 125.95, 123.44, 135.50 and 138.82 ppm as singlet peaks. It is noted that the strong peak at 123.44 ppm correspond to overlapped two carbons named C3 and C5 (Figure 3). Also, Ring A carbons (C1-C6) were calculated in the range of 144.43-121.98 ppm.

In addition to FT-IR and NMR analyses, molecular weight of title compound **(4)** was confirmed as 293.23 g/mol ($C_{13}H_9F_2N_3O_3$) with LC-MS analysis in negative and positive modes (see supplementary information).

Table 1. Comparison of the observed and calculated vibrational spectra of title compound.

Experimental		**Theoretical**		
Assignment	**Frequency (cm^{-1})**	**Frequency (cm^{-1})**	**Assignment PED (%)**	**Intensity (kcal/mol)**
urea N-H	3404	3476	*ν* NH 100	29
	3332	3318	*ν* NH 98	216
aromatic C-H streching	3127, 3098	3134	ν CH 99	22
		3126	ν CH 99	19
		3106	ν CH 95	4
		3102	ν CH 100	2
		3076	ν CH 96	11
		3066	ν CH 100	2
		3056	ν CH 93	7
urea C=O	1728	1714	ν OC 74	355
aromatic C=C	1605	1601	ν CC 45	298
aromatic C-H bending	1477, 1415	1211	ν NC 10+δ HCC 13+δ HCC 13	732
		1195	δ HCC 25+δ HCC 15+δ HCC 26	370
		1138	ν CC 12+δ HCC 15+δ HCC 40	1482
		1128	ν NC 14+ν NC 15+δ HCC 17+δ HCC 13	332
asymmetric NO_2	1502	1595	ν ON 10+ν CC 21+ν CC 10	272
		1541	ν ON 17+ν CC 14+ν ON 13+ν CC 11	151
		1435	ν ON 24+δ HNC 10+δ HCC 10	201
symmetric NO_2	1335	1313	ν ON 10+ν ON 21+ν NC 14	63
		1252	ν ON 22+ν CC 17+ ν NC 10	23
C-F	1113	1092	ν FC 25+ν FC 21+δ HCC 40	847
		985	ν CC 13+ν CC 11+ ν FC 16+δ HCC 12	75
		953	ν FC 12	11

ν: stretching, δ:in plane bending

Table 2. Theoretical and experimental ^{1}H and ^{13}C chemical shifts for 1-(3,5-difluorophenyl)-3-(2-nitrophenyl)urea.

^{1}H NMR			**^{13}C NMR**		
Assign.[a]	**Experimental[b] (ppm)**	**Calculated[c] (ppm)**	**Assign.[a]**	**Experimental[b] (ppm)**	**Calculated[c] (ppm)**
H2	8.18	9.37-7.16 (Ring A)	**C1**	134.63	140.17
H3	7.69		**C2**	125.95	130.57
H4	7.22		**C3, C5**	123.44[d]	124.22, 121.98
H5	8.06		**C4**	135.50	142.75
H9, H13	7.14	8.31-6.38 (Ring B)	**C6**	138.82	144.43
H11	6.82		**C7**	152.26	153.11
H(N2)	10.15	11.31	**C8**	142.50	146.96
H(N3)	9.60	6.31	**C9, C13**	101.97, 101.68	102.63, 102.59
			C10, C12	164.34[e], 161.92[e]	171.52, 170.83
			C11	98.01	100.02

a The assignments of atoms are according to the ORTEP numbering b NMR solvent: DMSO-d_6 c DFT/6-311G(d,p) d Overlapped e Average

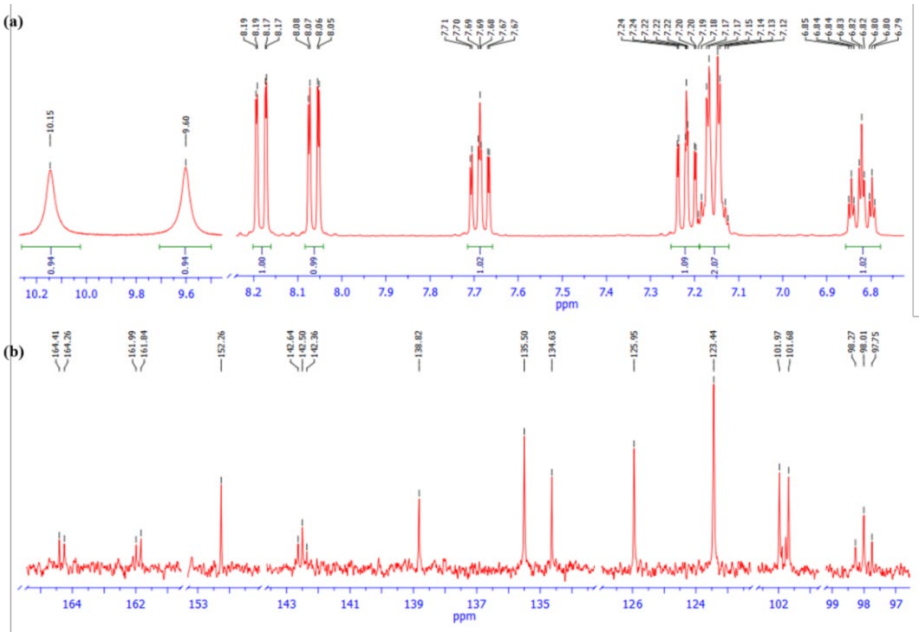

Figure 3. ^{1}H NMR (a) and ^{13}C NMR (b) spectra of compound **4.**

3.3. X-ray Crystal Structure of Compound 4

The molecular structure of compound **4** with the atom labeling was shown in Figure 4. The parameters for data collection and structure refinement of the compound were listed in Table 3. The nitro group is equivalent and typical of N=O double bonds [N1-O1=1.2184(19) Å and N1-O2=1.2277(19) Å]. The dihedral angle between phenyl rings is 35.62(5) °. The selected bond lengths and bond angles were given in Table 4. The molecules of **4** are connected by N-H···O hydrogen bonds (Table 5). Atom N3 atom acts as hydrogen-bond donor, via atom H3A, to nitro atom O2^{i} [(i) 1-x, -y, 1-z], forming a centrosymmetric $R_2^2(16)$ ring centered at (1/2, 0, 1/2). Compound **4** also contains two π···π interactions. The intermolecular π···π interactions occur between the two symmetry-related phenyl rings of neighboring molecules. The distances between the ring's centroids are 3.814 Å and 3.817 Å. The combination of π···π interactions produces one-dimensional supramolecular network which is running parallel to the [010] direction (Figure 5).

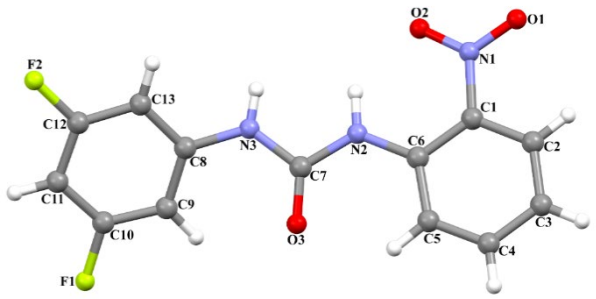

Figure 4. The molecular structure of **4** showing the atom numbering scheme.

3.4. Conformational Analysis

To determine stability of the molecule, 2D potential energy surface scanning (PES) was performed. Single point energies were calculated by changing θ_1(C6-N2-C14-S1) dihedral angle for -180˚/+180˚ angle range and 10˚ steps. As a result of PES (Figure 6) analysis, 4 conformations (Conf 1-4) corresponding to global and local minimum points were obtained. The molecular structures of these 4 conformations were optimized using DFT/B3LYP/6-311g (d, p) methods.

Table 3. Crystal data and structure refinement parameters for compound **4**.

Empirical formula	$C_{13}H_9F_2N_3O_3$
Formula weight	293.23
Crystal system	Monoclinic
Space group	I2/a
***a* (Å)**	25.8745 (16)
***b* (Å)**	3.8143 (3)
***c* (Å)**	24.7392 (19)
***β* (º)**	94.051 (6)°
***V* (Å^3)**	2435.5 (3)
Z	8
***D*$_c$ (g cm^{-3})**	1.599
μ (mm^{-1})	0.14
θ range (º)	4.4-28.1
Measured refls.	4365
Independent refls.	2391
***R*$_{int}$**	0.015
S	1.03
R1/wR$_2$	0.043/0.110
Δρ$_{max}$/Δρ$_{min}$ (eÅ^{-3})	0.23/-0.23

Celal Bayar University Journal of Science
Volume 17, Issue 3, 2021, p 285-295
Doi: 10.18466/cbayarfbe.887714

Table 4. Selected bond distances and angles for compound **4** (Å, º).

N1-O1	1.2184 (19)	N1-O2	1.2277 (19)
C7-O3	1.2029 (19)		
N3-C7-N2-C6	176.09 (18)	N2-C7-N3-C8	-176.24 (18)

Table 5. Hydrogen bonds parameters for compound **4** (Å, °).

D-H···A	D-H	H···A	D···A	D-H···A
N2—H2A···O2	0.88 (2)	1.95 (2)	2.6383 (18)	133
C5—H5···O3	0.93	2.18	2.811 (2)	124
N3—H3A···O2^{i}	0.83 (2)	2.55 (2)	3.2824 (19)	148

As seen in Table 6, conf 1 and conf 4 are the most stable structures. Hence, theoretical calculations were continued with the conf 1 structure (Figure 7).

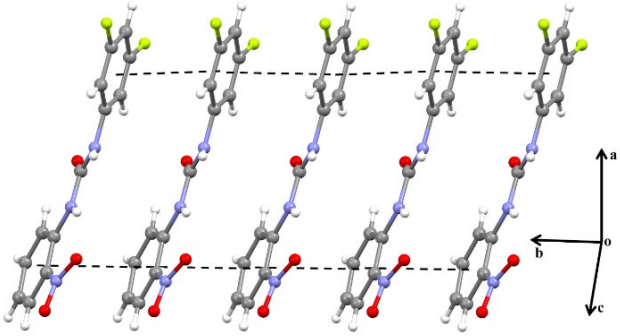

Figure 5. Crystal structure of **4**, showing the formation of a chain along [010] generated by π···π interactions.

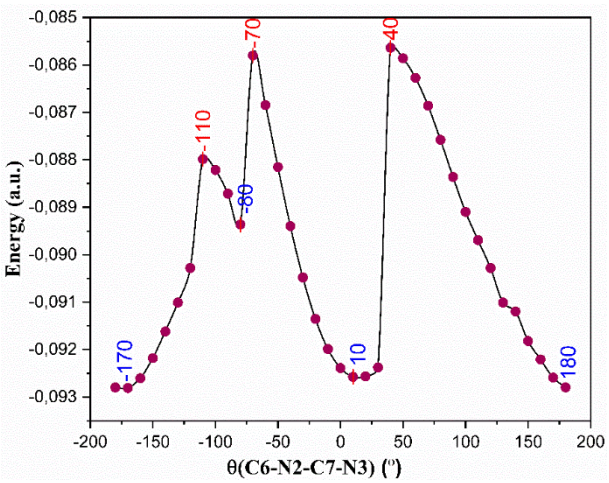

Figure 6. Molecular energy profile versus the selected torsional degree of freedom.

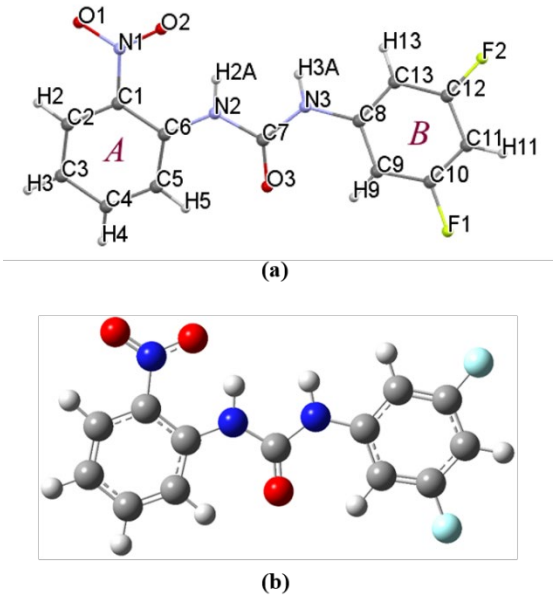

(a)

(b)

Figure 7. The X-ray (a) and optimized (b) structure (conf1) of the title compound.

Table 6. Conformation structures of the title molecule.

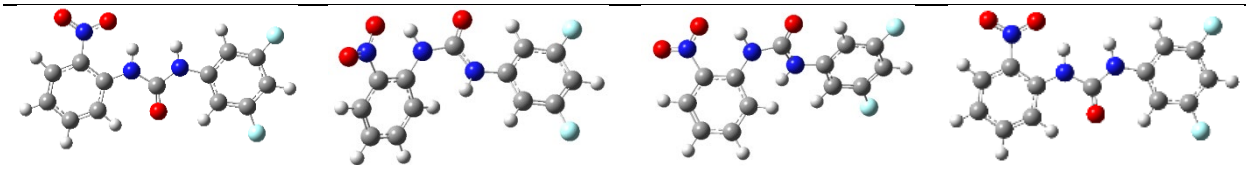

E= -1090.629173	E= -1090.621512	E= -1090.621512	E= -1090.629173
Conf1	Conf2	Conf3	Conf4

3.5. Frontier Molecular Orbitals

The Density-of-States (DOS) is an important concept in solid state physics and describes the number of states that are to be occupied by the system at each level of energy. The s, p, d atomic orbitals forming the molecule and Total Density-of-States (TDOS) were shown in Figure 8a. It was observed that atomic orbitals consist mainly of s and p orbitals. Besides, atomic orbital contributions of fragments are also shown in Figure 8b. It is also seen that the most contribution to the formation of molecular orbitals was provided by fragment 1 and fragment 2.

Celal Bayar University Journal of Science
Volume 17, Issue 3, 2021, p 285-295
Doi: 10.18466/cbayarfbe.887714

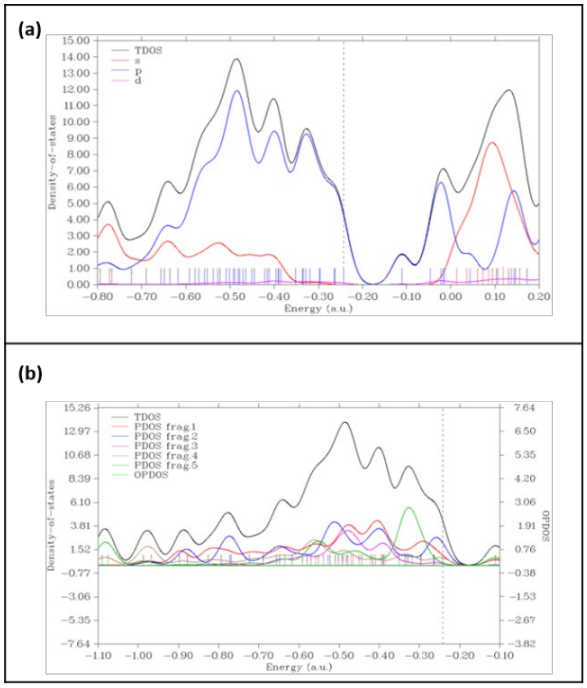

frag. 1: A ring; frag. 2: B ring; frag. 3: Cl1 and Cl 2 atoms; frag. 4: N1, N2 and N3 atoms; frag. 5: O1, O2 and O3 atoms

Figure 8. Plot TDOS, PDOS and OPDOS a) s, p and d orbitals b) specific fragments.

The frontier molecular orbitals (HOMO and LUMO) are the most important molecular orbitals. HOMO is molecular orbital of the highest energy that is occupied by electrons, while LUMO is the molecular orbital of the lowest energy that is not occupied by electrons. HOMO and LUMO orbitals of a molecule are also known as electron donor and acceptor groups [43-46]. They can be used to determine intermolecular charge transfers. Besides, molecular properties such as ionization potential, electron affinity, chemical reactivity, kinetic stability, polarization, conjugation can be calculated by considering these orbitals [47-50].

Figure 9 contains the orbital distributions of HOMO, HOMO-1, LUMO and LUMO+1 of the molecule. The highest 5 atomic contributions to these orbitals were calculated as LUMO + 1: C3 (16%) + C5 (14%) + C2 (12%) + C6 (12%) + C7 (12%), LUMO: N1 (26%) + O1 (21%) + O2 (19%) + C4 (10%) + C2 (9%), HOMO: N2 (10%) + N3 (18%) + C3 (7%) + C11 (18%) + C5 (5%), HOMO- 1: C13 (25%) + C10 (15%) + C9 (10%) + C12 (6%) + C3 (5%). As can be seen, these 5 atoms are expected to be the most active in a reaction or interaction in the HOMO, HOMO-1, LUMO and LUMO + 1 orbitals of the title compound.

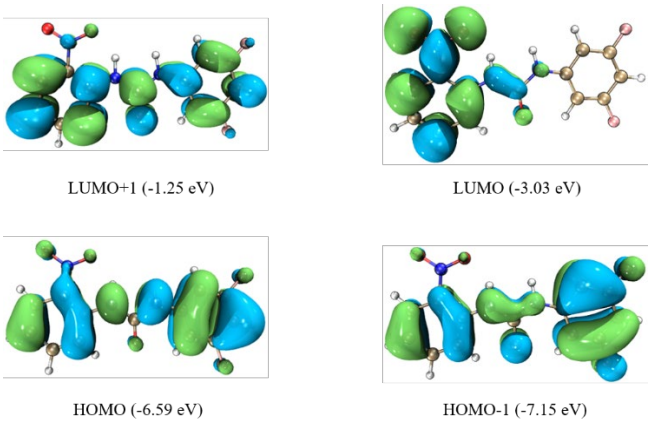

Figure 9. Molecular orbital surfaces and energy levels.

3.6. AIM Charge and MEP Analyzes

Bader's QTAIM theory has been used for details about the nature and strength of intra- and inter-molecular hydrogen bonds [51]. The strength and interaction type of the intra- and inter-molecular bonds in the compound were obtained by using the electron density(ρ_{BCP}), the Laplacian of electron density ($\nabla^2(\rho_{BCP})$), the potential energy density (V(r)), the kinetic energy density (G (r)) and electronic energy density (H (r)) in the BCPs (different bond critical points). $\nabla^2(\rho_{BCP})$ is negative in covalent bonds, while it is positive in the bonds formed by ionic, Van der Waals and hydrogen interactions. Rozas et al. [52] evaluated that $\nabla^2(\rho_{BCP}) < 0$ and $H_{BCP} < 0$ for the strong hydrogen bonds that have covalent character, $\nabla^2(\rho_{BCP}) > 0$ and $H_{BCP} < 0$ for the medium-strong hydrogen interactions that have partial covalent character, and

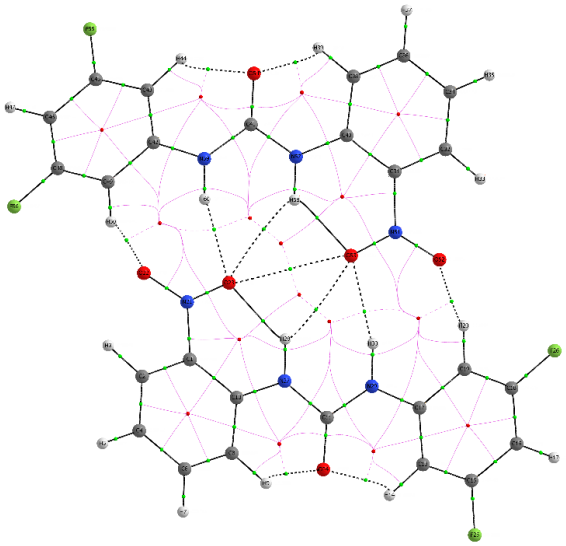

Figure 10. Molecular graph of dimer: bond critical points (small green spheres), ring critical points (small red sphere).

$\nabla^2(\rho_{BCP}) > 0$ and $H_{BCP} > 0$ for the weak hydrogen bonds that have electrostatic character. The molecular graph of the compound's dimer structure is shown in Figure 10.

Table 7 shows the intra-molecular and inter-molecular interactions observed in the molecule. Interaction energies (E_{int}) were calculated to determine the significances of these interactions. The relationship between E_{int} and potential energy density was given as E_{int}= 1/2 (V_{BCP}) by Espinoza [53]. In Table 7, it was found that the interaction energy of the N2-H2A···O2 hydrogen bond is greater than other interactions (E_{int}= -9.37 kcal/mol). The positive $\boldsymbol{\rho_{BCP}}$ and $\boldsymbol{H_{BCP}}$ values of the three interactions also showed that these interactions are weak hydrogen bonds that have electrostatic character.

Table 7. Topological parameters for bonds of interacting atoms.

Interaction	ρ_{BCP} (a.u.)	$\nabla^2\rho_{BCP}$ (a.u.)	G_{BCP} (a.u.)	V_{BCP} (a.u.)	H_{BCP} (a.u.)	E_{int} (kcal/mol)
N2-H2A…O2	+0.034478	+0.133038	+0.031571	-0.029883	+0.001688	-9.37
N2-H2A…O2^{i}	+0.007258	+0.028038	+0.005847	-0.004685	+0.001162	-1.47
N3-H3A…O2^{ii}	+0.016754	+0.056357	+0.012333	-0.010576	+0.001757	-3.32

H(r) = G(r) + V(r)

When the molecular electrostatic potential (MEP) map (Figure 11) of the optimized molecule is examined, the regions coded with red (the most negative region) and blue (the most positive region) are clearly visible. As can be seen in Figure 11, negative regions in the molecule were found around the O1, O2, O3, F1 and F2 atoms. The most negative region was found around the O1 (MEP value is -0.036 a.b.). MEP values for O2, O3, F1 and F2 atoms are -0.031, -0.030, -0.021 and -0.018 a.b., respectively. According to this result, these five atoms are the most suitable regions for electrophilic attack reaction. The positive regions in MEP map were localized on the hydrogen atoms. The most positive region for the nucleophilic attack is around the H3A atom and the MEP value is defined as +0.067 a.b.

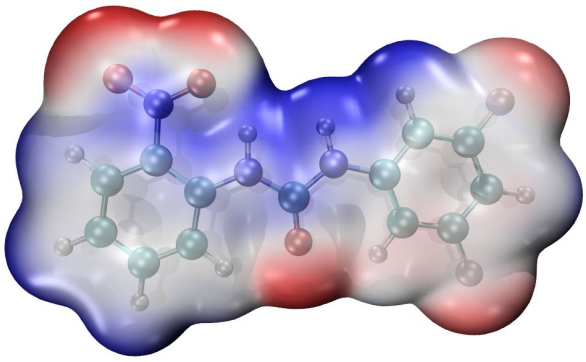

Figure 11. MEP surface obtained from the electron density of the title compound.

In particular, O1 and O2 atoms to LUMO orbitals, N2 and N3 atoms also contribute to HOMO orbitals in Figure 9 and these atoms are in the most negative and positive region in the MEP map. These two situations show the congruence of molecular orbitals and MEP calculations.

4. Conclusion

In summary, the target compound, 1-(3,5-difluorophenyl)-3-(2-nitrophenyl) urea was successfully synthesized in 92% yield using 2-nitroaniline, 3,5-difluoroaniline and triphosgene as readily available starting materials with two-step synthesis method. The orange crystals of product were grown by the slow evaporation technique using THF and ethyl acetate solvent system as inner and outer solvent, respectively. The obtained crystals were identified by various characterization techniques such as melting point, FT-IR, ^{1}H NMR, ^{13}C NMR, MS and X-ray single diffraction analysis. Besides, calculated IR and NMR results were given by comparing to experimental results. Slight differences were observed because the experimental results were obtained at the solid phase and in silico calculations pertain to the gaseous phase. To determine the stability of the molecule, 2D potential energy surface scanning (PES) was performed. As a result of PES analysis, the most stable conformations were obtained and compared with X-ray structure of compound. Frontier molecular orbitals and MEP analyzes of the optimized structure were calculated. Molecular electrostatic potential confirm the compound electrophile and nucleophile attack of the reactive centers. According to the MEP map, the most negative and positive regions of the molecule were determined. We hope the results of this study will help the researchers to analyze and synthesize new materials.

Acknowledgement

T. Güngör wish to thank Dr. Mehmet AY and Dr. Fatma Aydın for their support.

Author's Contributions

Tuğba Güngör: Designed all study, performed the synthesis and characterization studies, interpreted the results and wrote the manuscript.
Tuncay Karakurt: Performed the theoretical studies and wrote the manuscript.
Z. Sibel Şahin: Performed the X-ray and conformational analysis and wrote the manuscript.

Ethics

There are no ethical issues after the publication of this manuscript.

Supplementary Information

Supplementary data consists of all characterization data of the product. Crystallographic data for the structural analysis has been deposited with the Cambridge Crystallographic Data Centre, CCDC No. 2009298. Copies of this information may be obtained free of charge from the Director, CCDC, 12 Union Road, Cambridge CB2 1EZ, UK (fax: +44-1223-336033; e-mail: deposit@ccdc.cam.ac.uk or www: http://www.ccdc.cam.ac.uk).
For Supporting Information:
http://fbe.mcbu.edu.tr/db_images/file/T.Gungor-supporting_information.pdf

References

1. Al-Masoudi, NA, Essa, AH, Alwaaly, AAS, Saeed, BA, Langer, P. 2017. Synthesis and conformational analysis of new arylated-diphenylurea derivatives related to sorafenib drug via Suzuki-Miyaura crosscoupling reaction. *Journal of Molecular Structure*; 1146: 522-529.

2. Atahan, A, Gencer, N, Bilen, Ç, Yavuz, E, Genç, H, Sonmez, F, Zengin, M, Ceylan, M, Kucukislamoglu, M. 2018. Synthesis, biological activity and structure-activity relationship of novel diphenylurea derivatives containing tetrahydroquinoline as carbonic anhydrase I and II inhibitors. *ChemistrySelect*; 3: 529-534.

3. Strumberg, D, Schultheis, B. 2012. Regorafenib for cancer. Expert Opinion on Investigational Drugs; 21(6): 879-889.

4. Ruan, BF, Lin, MX, Shao, Q, Wang, TH, Zhang, Q, Dong, Y, Bu, C, Xu, H, Zhou, B, Li, Q. 2018. Modification, biological evaluation and SAR studies of novel 1H-Pyrazol derivatives containing N,Nı-disubstituted urea moiety as potential anti-melanoma agents. *Chemistry & Biodiversity;* 15: 1700504, 1-9.

5. Gentile, C, Martorana, A, Lauria, A, Bonsignore, R. 2017. Kinase inhibitors in multitargeted cancer therapy. *Current Medicinal Chemistry*; 24: 1671-1686.

6. Bobrovs, R, Jaudzems, K, Jirgensons, A. 2019. Exploiting structural dynamics to design open-flap inhibitors of malarial aspartic proteases. *Journal of Medicinal Chemistry*; 62: 8931-8950.

7. Zhang, Y, Anderson, M, Weisman, JL, Lu, M, Choy, CJ, Boyd, VA, Price, J, Sigal, M, Clark, J, Connelly, M et al. 2010. Evaluation of diarylureas for activity against Plasmodium falciparum. *ACS Medicinal Chemistry Letters*; 1: 460-465.

8. Huang, W, Lv, D, Yu, H, Sheng, R, Kim, SC, Wu, P, Luo, K, Li, J, Hu, Y. 2010. Dual-target-directed 1,3-diphenylurea derivatives: BACE 1 inhibitor and metal chelator against Alzheimer's disease. *Bioorganic & Medicinal Chemistry*; 18: 5610-5615.

9. Tang, C, Loeliger, E, Kinde, I, Kyere, S, Mayo, K, Barklis, E, Sun, Y, Huang, M, Summers, MF. 2003. Antiviral inhibition of the HIV-1 capsid protein. *Journal of Molecular Biology*; 327: 1013-1020.

10. Biswal, BK, Morisseau, C, Garen, G, Cherney, MM, Garen, C, Niu, C, Hammock, BD, James, MNG. 2008. The molecular structure of epoxide hydrolase B from Mycobacterium tuberculosis and its complex with a urea-based inhibitor. *Journal of Molecular Biology*; 381: 897-912.

11. Sikka, P, Sahu, JK, Mishra, AK, Hashim, SR. 2015. Role of Aryl Urea Containing Compounds in Medicinal Chemistry. *Medicinal Chemistry*; 5(11): 479-483.

12. Perveen, S, Mustafa, S, Khan, MA, Dar, A, Khan, KM, Voelter, W. 2012. Substituted urea derivatives: a potent class of antidepressant agents. *Medicinal Chemistry*; 8: 330-336.

13. Carra, A, Del Signore, MB, Sottile, F, Ricci, A, Carimi, F. 2012. Potential use of new diphenylurea derivatives in micropropagation of Capparis spinosa L. Plant Growth Regulation; 66: 229-237.

14. Bigi, F, Maggi, R, Sartori, G. 2000. Selected syntheses of ureas through phosgene substitutes. *Green Chemistry*; 2(4): 140-148.

15. Asakawa, C, Ogawa, M, Fujinaga, M, Kumata, K, Xie, L, Yamasaki, T, Yui, J, Fukumura, T, Zhang, M. 2012. Utilization of [11C] phosgene for radiosynthesis of N-(2-{3-[3,5-bis(trifluoromethyl)]phenyl[11C]ure2;ido}ethyl)glycyrrhetinamid, an inhibitory agent for proteasome and kinase in tumors. *Bioorganic & Medicinal Chemistry Letters*; 22(11): 3594-3597.

16. Majer, P, Randad, RS. 1994. A Safe and Efficient Method for Preparation of N,N'-Unsymmetrically Disubstituted Ureas Utilizing Triphosgene. *Journal of Organic Chemistry*; 59: 1937-1938.

17. Artuso, E, Degani, I, Fochi, R, Magistris, C. 2007. Preparation of Mono-, Di-, and Trisubstituted Ureas by Carbonylation of Aliphatic Amines with S,S-Dimethyl Dithiocarbonate. Synthesis; 22: 3497-3506.

18. Katritzky, AR, Pleynet, DPM, Yang, B. 1997. A General Synthesis of Unsymmetrical Tetrasubstituted Ureas. *Journal of Organic Chemistry*; 62: 4155-4158.

19. Sonoda, N. 1993. Selenium assisted carbonylation with carbon monoxide. *Pure & Applied Chemistry*; 65(4): 699-706.

20. Shi, F, Deng, Y, SiMa, T, Peng, J, Gu, Y, Qiao, B. 2003. Alternatives to Phosgene and Carbon Monoxide: Synthesis of Symmetric Urea Derivatives with Carbon Dioxide in Ionic Liquids. Angewandte Chemie International Edition; 42: 3257-3260.

21. Semenov, AV, Tarasova, IV, Khramov, VS, Semenova, EV, Inchina, VI, Vakaeva, SS. 2018. Glucokinase activators based on N-Aryl-Nı-Pyridin-2-ylurea derivatives. *Pharmaceutical Chemistry Journal*; 52(3): 209-212.

22. Sheldrick, GM. 2008. A short history of SHELX. Acta Crystallographica Section A; A64: 112-122.

23. Sheldrick, GM. 2015. Crystal structure refinement with SHELXL. Acta Crystallographica Section C; C71: 3-8.

24. APEX2, Bruker AXS Inc. Madison Wisconsin USA (2013).

25. Macrae, CF, Sovago, I, Cottrell, SJ, Galek, PTA, McCabe, P, Pidcock, E, Platings, M, Shields, GP, Stevens, JS, Towler, M et al. 2020. Mercury 4.0: From visualization to analysis, design and prediction. *Journal of Applied Crystallography*; 53: 226-235.

26. Farrugia, LJ. 2012. WinGX and ORTEP for Windows: an update. *Journal of Applied Crystallography*; 45: 849-854.

27. Becke, AD. 1993. Density–functional thermochemistry. III. The role of exact exchange. *The Journal of Chemical Physics*; 98: 5648–5652.

28. Lee, C, Yang, W, Parr, RG. 1988. Development of the Colle–Salvetti correlation–energy formula into a functional of the electron density. *Physical Review B*; 37: 785.

29. Foresman, JB, Frisch, A. Exploring chemistry with electronic structure methods: a guide to using Gaussian, 1996.

30. Frisch, M, Trucks, G, Schlegel, HB, Scuseria, G, Robb, M, Cheeseman, JR, Scalmani, G, Barone, V, Petersson, GA, Nakatsuji, H, et al. Gaussian 09, revision a. 02, Gaussian. Inc., Wallingford, CT, 200, 2009.

31. Keith, TA, AIMAll (Version 15.09.27), T.K. Gristmill Software, Overland Park K.S., USA, 2016.

32. Lu, T, Chen, F. 2012. Multiwfn: A multifunctional wavefunction analyzer. *Journal of Computational Chemistry*; 33(5): 580-592.

33. Çukurovalı, A, Karakurt, T. 2019. Synthesis, spectroscopic, X-ray diffraction and tautomeric properties of 5-(diethylamino)-2-((2-(5-(3-methyl-3-phenylcyclobutyl)-6H-1,3,4-thiadiazin-2-yl) hydrazono)methyl)phenol: A combined experimental and theoretical study. *Journal of Molecular Structure*; 1189: 328-337.

34. Karakurt, T, Çukurovalı, A, Subaşı, NT, Kani, I. 2016. Molecular structure and computational studies on 2-((2-(4-(3-(2,5-dimethylphenyl)-3-methylcyclobutyl)thiazol-2-yl)hydrazono) methyl)phenol monomer and dimer by DFT calculations. *Journal of Molecular Structure*; 1125: 433-442.

35. Karakurt, T, Çukurovalı, A, Subaşı, NT, Onaran, A, Ece, A, Eker, S, Kani, I. 2018. Experimental and theoretical studies on tautomeric structures of a newly synthesized 2,2'(hydrazine-1,2-diylidenebis(propan-1-yl-1-ylidene))diphenol. *Chemical Physics Letters*; 693: 132-145.

36. Karakurt, T, Çukurovalı, A, Kani, İ. 2020. Structure of 2-(2-(anthracen-9-ylmethylene) hydrazinyl)-4-(3-methyl-3-phenylcyclobutyl)thiazole by combined X-Ray crystallographic and molecular modelling studies. *Molecular Physics*; 1-17.

37. Varsányi, G. Assignments for Vibrational Spectra of Seven Hundred Benzene Derivatives, Halsted Press, 1974.

38. Furic, K, Mohacek, V, Bonifacic, M, Štefanic, I. 1992. Raman spectroscopic study of H2O and D2O water solutions of glycine. *Journal of Molecular Structure*; 267: 39-44.

39. Avcı, D, Atalay, Y, Şekerci, M, Dinçer, M. 2009. Molecular structure and vibrational and chemical shift assignments of 3-(2-hydroxyphenyl)-4-phenyl-1H-1,2,4-triazole-5-(4H)-thione by DFT and ab initio HF calculations. *Spectrochimica acta. Part A, Molecular and Biomolecular Spectroscopy*; 73: 212-217.

40. Mohan, Organic Spectroscopy: Principles and Applications, Crc Press, 2004.

41. Ditchfield, R. 1972. Molecular Orbital Theory of Magnetic Shielding and Magnetic Susceptibility. *The Journal of Chemical Physics*; 56: 5688-5691.

42. Wolinski, K, Hinton, JF, Pulay, P. 1990. Efficient implementation of the gauge-independent atomic orbital method for NMR chemical shift calculations. *Journal of American Chemical Society*; 112(23): 8251-8260.

43. Fukui, K. 1982. Role of frontier orbitals in chemical reactions. *Science*; 218: 747-754.

44. Büyükuslu, H, Akdoğan, M, Yıldırım, G, Parlak, C. 2010. Ab initio Hartree–Fock and density functional theory study on characterization of 3-(5-methylthiazol-2-yldiazenyl)-2-phenyl-1H-indole. *Spectrochimica Acta Part A: Molecular and Biomolecular Spectroscopy*; 75: 1362-1369.

45. Chaudhary, T. Chaudhary, MK. Joshi, BD. Santana, MSA. Ayala, AP. 2021. Spectroscopic (FT-IR, Raman) analysis and computational study on conformational geometry, AIM and biological activity of cephalexin from DFT and molecular docking approach. *Journal of Molecular Structure*; 1240: 130597.

46. Al-Otaibi, JS. Mary, YS. Armaković, S. Thomas, R. 2020. Hybrid and bioactive cocrystals of pyrazinamide with hydroxybenzoic acids: detailed study of structure, spectroscopic characteristics, other potential applications and noncovalent interactions using SAPT. *Journal of Molecular Structure*, 1202: 127316.

47. Parr, RG, Pearson, RG. 1983.Absolute hardness: companion parameter to absolute electronegativity. *Journal of the American Chemical Society*; 105: 7512-7516.

48. Parr, RG, Donnelly, RA, Levy, M, Palke, WE. 1978. Electronegativity: the density functional viewpoint. *The Journal of Chemical Physics*; 68: 3801-3807.

49. Parr, RG, Szentpály, LV, Liu, S. 1999. Electrophilicity index. *Journal of the American Chemical Society*; 121: 1922-1924.

50. Jeelani, A. Muthu, S. Narayana, B. 2021. Molecular structure determination, Bioactivity score, Spectroscopic and Quantum computational studies on (E)-N'-(4-Chlorobenzylidene)-2-(napthalen-2-yloxy) acetohydrazide. *Journal of Molecular Structure*; 1241: 130558.

51. Bader, RFW. 2006. Pauli Repulsions Exist Only in the Eye of the Beholder. *Chemistry-A European Journal*; 12(10): 2896-2901.

52. Rozas, I, Alkorta, I, Elguero, J. 2000. Behavior of Ylides Containing N, O, and C Atoms as Hydrogen Bond Acceptors. *Journal of the American Chemical Society*; 122(45): 11154-11161.

53. Espinosa, E, Molins, E, Lecomte, C. 1998. Hydrogen bond strengths revealed by topological analyses of experimentally observed electron densities. *Chemical Physics Letters*; 285(3): 170-173.